

Document downloaded from:

<http://hdl.handle.net/10251/144830>

This paper must be cited as:

Ibanez, J.; Blazquez, O.; Hernandez, S.; Garrido, B.; Rodríguez-Hernández, P.; Muñoz, A.; Velazquez, M.... (16-1). Lattice dynamics study of cubic Tb₂O₃. *Journal of Raman Spectroscopy*. 49(12):2021-2027. <https://doi.org/10.1002/jrs.5488>



The final publication is available at

<https://doi.org/10.1002/jrs.5488>

Copyright John Wiley & Sons

Additional Information

"This is the peer reviewed version of the following article: Ibáñez, Jordi, Oriol Blázquez, Sergi Hernández, Blas Garrido, Plácida Rodríguez-Hernández, Alfonso Muñoz, Matias Velázquez, Philippe Veber, and Francisco Javier Manjón. 2018. Lattice Dynamics Study of Cubic Tb₂O₃. *Journal of Raman Spectroscopy* 49 (12). Wiley: 2021 27. doi:10.1002/jrs.5488, which has been published in final form at <https://doi.org/10.1002/jrs.5488>. This article may be used for non-commercial purposes in accordance with Wiley Terms and Conditions for Self-Archiving."

Lattice dynamics study of bixbyite-type Tb₂O₃

J. Ibáñez,^{1*} O. Blázquez,² S. Hernández,² B. Garrido,² P. Rodríguez-Hernández,³ A. Muñoz,³ Ph. Veber,^{4,5} M. Velázquez,⁴ and F. J. Manjón^{6*}

¹*Institute of Earth Sciences Jaume Almera (CSIC), Lluís Solé i Sabarís s/n, 08028 Barcelona, Catalonia, Spain*

²*MIND-IN₂UB, Departament d'Electrònica, Universitat de Barcelona, Martí i Franquès 1, 08028 Barcelona, Catalonia, Spain*

³*Departamento de Física, Instituto de Materiales y Nanotecnología, MALTA Consolider Team, Universidad de La Laguna, 38207 San Cristóbal de la Laguna, Tenerife, Spain*

⁴*CNRS, Université de Bordeaux, ICMCB, UPR 9048, 33608 Pessac cedex, France*

⁵*Université Lyon, Université Claude Bernard Lyon 1, CNRS, Institut Lumière Matière UMR 5306, F-69100, Villeurbanne, France*

⁶*Instituto de Diseño para la Fabricación y Producción Automatizada, MALTA Consolider Team, Universitat Politècnica de València, 46022 València, Spain*

* corresponding authors: jibanez@ictja.csic.es; fjmanjon@fis.upv.es

Abstract

We report a joint experimental and theoretical study of the lattice dynamics of Tb₂O₃. Polarized and unpolarized Raman-scattering measurements of a high-quality Tb₂O₃ single crystal have been performed at both low and room temperatures. Up to sixteen Raman-active modes have been observed, and the measured phonon frequencies have been compared with those of other rare-earth (RE) and related sesquioxides with C-type or bixbyite structure. The comparison between our measurements and the results of first-principles calculations allow us to correctly assign the symmetry of the experimentally observed Raman-active modes. Additional lattice-dynamical calculations of the related RE sesquioxides Dy₂O₃, Gd₂O₃, Eu₂O₃ and Sm₂O₃ indicate that the Raman frequencies of these compounds are monotonically reduced with increasing the lattice parameter along the Dy₂O₃-Tb₂O₃-Gd₂O₃-Eu₂O₃-Sm₂O₃ series, thus prompting for a revision of the experimental Raman spectra of some of these compounds (mainly Eu₂O₃, but also Gd₂O₃).

1- Introduction

Rare-earth (RE) sesquioxides (R_2O_3 , $R = Y, Sc$, or lanthanide) are interesting materials due to their remarkable fundamental properties and potential applications. These compounds may enable a wide range of technological advances including light emitters, catalysts, or high-dielectric constant (high-k) gates. Among this family of compounds, terbium oxide (Tb_2O_3) has attracted considerable attention in the last few years as a high-k material [JAP_2010,TSF_2012,APL_2014] and also as an active material for high-performance optoelectronic devices.[Geppert,Belaya,Bakovets] Recently, it has been shown that millimeter-sized C-type Tb_2O_3 pure single crystals can be grown with a controlled atmosphere flux method, using melting temperatures much lower than those of pure Tb_2O_3 . [CEC_2015] The high-quality cubic Tb_2O_3 crystals thus obtained are highly promising for applications in optics and photonics.

It is well-known that, depending on the RE ionic radius and temperature, R_2O_3 compounds may exhibit different polymorphic modifications. These may be cubic (C phase), monoclinic (B phase) or hexagonal (A phase). The C-type (or bixbyite) structure with space group $Ia-3$, No. 206, is usually the stable phase at room temperature in the case of the heavier lanthanides, like Tb_2O_3 , and also in related sesquioxides like Mn_2O_3 , In_2O_3 and Tl_2O_3 . In addition, different stoichiometries can be grown due to different oxidation states of the RE cation. This is particularly relevant for the binary Tb oxides, where Tb^{3+} and Tb^{4+} states coexist and therefore different TbO_x compounds with $1.5 < x < 2$ are usually formed. Thus, it is highly important to properly characterize the as-grown RE oxide samples in order to identify the co-existing phases and stoichiometries.

Raman scattering (RS) is a powerful nondestructive analytical tool that provides useful information, among others, about the crystal quality, structural properties and lattice dynamics of solid-state materials. Many different studies have been devoted to investigate the RS properties of C-type RE sesquioxides (see Ref. [Abrashv] and references therein) or their solid solutions.[Irshad] It is now clear that the high-frequency Raman peaks, involving mainly O vibrations, of C-type R_2O_3 compounds basically display a monotonic behavior as a function of the lattice parameter. In turn, the frequency of the low-frequency modes involving lanthanide vibrations is almost constant for the whole family of R_2O_3 compounds, except Sc_2O_3 and Y_2O_3 due to the much smaller mass of the R ion.[Abrashv] However, there are still open questions in relation to the vibrational properties of these compounds. For instance, cubic Eu_2O_3 seems to exhibit an anomalous behavior (softening) that has been ascribed to either the presence of oxygen vacancies or to the specific electronic structure of Eu^{3+} relative to the rest of lanthanides.[Abrashv] Additionally, the information about Tb_2O_3 is still scarce in spite of the large number of papers devoted to the RS properties of R_2O_3 compounds.[Urban]

The aim of the present work is to investigate the lattice-dynamical properties of Tb_2O_3 . For this purpose, we have performed RS measurements on a high-quality Tb_2O_3 single crystal. Polarized Raman spectra, in combination with first-principles DFT calculations of the zone-center phonons, have allowed us to unambiguously identify the first-order Raman peaks of Tb_2O_3 . The DFT calculations are extended to other R_2O_3 compounds ($\text{R} = \text{Sm}, \text{Eu}, \text{Gd}, \text{Dy}$), which allows us to shed additional light on the possible anomalous behavior of the lattice dynamics in these compounds, like that observed in Eu_2O_3 .

2- Methods

Cubic Tb_2O_3 single crystals were grown by a controlled atmosphere flux method using a $\text{Li}_6\text{Tb}(\text{BO}_3)_3$ solvent and Tb_2O_3 as the solute. The flux solution was melted at 1230 °C (less than half the melting temperature of Tb_2O_3) and subsequently cooled down slowly to 1160 °C. After cutting and polishing, almost inclusion-free, millimeter-sized crystals oriented along the [112] direction were obtained. Details of the growth method can be found in Ref. [CEC_2015].

Room-temperature polarized and unpolarized micro-RS measurements were excited with the 532-nm line of a solid state laser. Inelastically scattered light was collected with a Horiba Jobin Yvon LabRAM HR spectrometer equipped with an edge filter that cuts Raman signals below $\sim 50 \text{ cm}^{-1}$ and a thermoelectrically cooled multichannel CCD detector enabling a spectral resolution better than 2 cm^{-1} . Unpolarized RS measurements were also performed at 80 K by using a Linkam microscope stage. Different Raman spectra were acquired at various sample orientations, relative to the polarization of the incoming light, by rotating the sample around the [112] direction (i.e., the crystal orientation). These measurements allowed us to properly identify all the features that appear in the Raman spectra of Tb_2O_3 .

3- DFT calculations

Ab initio total-energy calculations for the C-type structure of the RE sesquioxides (Tb_2O_3 , Dy_2O_3 , Gd_2O_3 , Eu_2O_3 and Sm_2O_3) were carried out within the framework of density functional theory (DFT). The Vienna Ab-initio Simulation Package (VASP) [VASP] was used to perform calculations with the pseudopotential method and the projector augmented waves (PAW) scheme. The exchange-correlation energy was obtained in the generalized gradient approximation (GGA) using the PBE prescription [PBE] and its extension to the solid state, PBEsol. [PBEsol] A dense $X \times X \times X$ Monkhorst–Pack grid of special k-points and a plane-wave basis set with energy cutoffs of 520 eV were used.

Table I shows the resulting ambient-pressure lattice parameter (a_0), zero-pressure bulk modulus (B_0) and first-derivative of the bulk modulus (B') obtained for Tb_2O_3 , both with PBE and PBEsol functionals, after the full structural relaxation of its cubic crystal lattice. The corresponding B_0 and B' values were obtained with a fit to the P - V data obtained during the structural relaxation, using a 3rd-order Birch-Murnaghan equation of state. In the relaxed optimized configurations, the resulting forces on the atoms are less than ??? eV/Å, with deviations of the stress tensor from hydrostatic conditions (diagonal tensor) lower than 0.1 GPa. As can be seen in **Table I**, the lattice parameter calculated with both PBE and PBEsol differs by less than ~1% with respect to the experimental data. However, the PBE value is much closer to the experimental value. Owing to this, the larger lattice spacing obtained with PBE gives rise to a sizably larger compressibility relative to PBEsol (see **Table I**). Although the theoretical PBE lattice parameter is in better agreement with the experimental value, in the present work we rely on the PBEsol functional since, as will be shown below (and as also found in other related compounds like C-type In_2O_3 [García-Domene12]), it provides much better results in the case of the lattice-dynamical calculations.

The elastic constants of C-type Tb_2O_3 were also calculated within DFT-PBEsol as implemented in VASP. Details of *ab initio* calculations of the mechanical properties of isostructural sesquioxides can be found elsewhere.[Gomis14] The following values were obtained for the three independent elastic constants of the cubic lattice of Tb_2O_3 : $C_{11}= 221.62$ GPa, $C_{12}=116.52$ GPa and $C_{44}=72.67$ GPa. The bulk modulus can then be independently obtained using the expression $B_0=(C_{11}+2C_{12})/3$ for materials with cubic symmetry. This formula gives a value of 151.5 GPa for Tb_2O_3 , which is in very good agreement with the value obtained after the structural relaxation ($B_0=151.24$ GPa, see **Table I**), showing the consistency of the present calculations.

Lattice-dynamics calculations were performed for Dy_2O_3 , Tb_2O_3 , Gd_2O_3 , Eu_2O_3 and Sm_2O_3 . Phonon frequencies for all these compounds were calculated at the Γ point using the direct-force constant approach as implemented in VASP, using the PBEsol functional to compute the atomic forces. For comparison purposes, the Γ -point phonon frequencies of Tb_2O_3 were also obtained using the PBE functional. For this compound, the calculations were also carried out along high-symmetry directions of the Brillouin zone, which allowed us to compute the phonon dispersion and one-phonon density of states (PDOS). We show in **Fig. 1** the Tb- and O-projected PDOS for cubic Tb_2O_3 . The figure clearly illustrates the fact that the optical phonons of Tb_2O_3 involving O (Tb) atoms have frequencies higher (lower) than 250 cm^{-1} (225 cm^{-1}), leaving a small bandgap around 25 cm^{-1} between both types of modes. Such bandgap is much larger in the case of the zone-center optical phonons. As can be seen in Fig. 2, the frequency of the Raman-active phonons of Tb_2O_3 involving Tb (O) vibrations is below (above) 200 cm^{-1} (300 cm^{-1}), yielding a bandgap larger than 100 cm^{-1} .

4- Results

As discussed in different previous works,[Abrashv,Todorov,White] C-type RE and related sesquioxides have 22 different Raman-active modes transforming as $\Gamma_{\text{Raman}}=4A_g + 4E_g + 14F_g$. Note that F_g modes are also noted T_g in many texts. **Figure 2** shows an unpolarized Raman spectrum of Tb_2O_3 obtained at 80 K together with the frequency position of the 22 Raman-active modes as obtained with DFT lattice-dynamical calculations, using the PBEsol functional. Up to 16 different modes are observed in the low-temperature spectrum (bands marked with an asterisk probably correspond to Tb-related photoluminescence emission, see below). This large number of measured modes is higher than that reported for most of the C-type sesquioxides. [Abrasev] However, it is similar to that recently obtained in related bixbyite-type sesquioxides like In_2O_3 . [García-Domene12, Kranert14]

A comparison between the calculated and experimental frequencies of the Raman-active optical phonons of Tb_2O_3 can be found in **Table II**. Band assignments are later confirmed in terms of additional Raman measurements with different scattering geometries. As can be seen in **Fig. 2** and in **Table II**, fairly good agreement is found between the calculated frequencies and the experimental position of most Raman peaks when the PBEsol functional is used. In contrast, the results obtained with the PBE functional (see also **Table II**) tend to underestimate the frequency of most optical phonon modes, especially those involving O vibrations. In general, PBEsol calculations in sesquioxides are found to provide fairly good results, and only provide a slight underestimation of the Raman frequencies observed at room conditions, as is the case of Tb_2O_3 in the present work and also as previously found in In_2O_3 . [García-Domene12]

As in the rest of C-type R_2O_3 sesquioxides,[Abrashv] the Raman spectrum of Tb_2O_3 is dominated by a strong peak corresponding to a F_g mode. This peak is located at $\sim 370 \text{ cm}^{-1}$ in the case of Tb_2O_3 . In contrast, some of the Raman-active modes are barely visible or, simply, do not show up in the spectra. In **Fig. 2**, the bands marked with an asterisk cannot be ascribed to first-order Raman scattering, since no phonon modes are expected in this frequency region, neither can they be assigned to second-order modes, owing to their temperature behavior. Indeed, Raman measurements acquired at different temperatures (not shown) revealed that the intensity of these features decreases with increasing temperature, which is opposite to the expected behavior for second-order modes. Most likely, these bands correspond to photoluminescence peaks arising from $^5\text{D}_4$ to $^7\text{F}_5$ intra-4f electronic radiative transitions in Tb^{3+} ions, the energy of which is just below 550 nm.[Zhong,Silversmith] Analogous conclusions have been reported for similar peaks detected in other R_2O_3 compounds. [Jinqiu]

The single crystal studied in this work allowed us to carry out polarized RS measurements. Such measurements, in combination with the results of the DFT calculations, are helpful to confirm the

assignments of the different peaks that show up in the unpolarized Raman spectra. **Figure 3** shows two different room-temperature Raman spectra of Tb_2O_3 obtained in parallel and perpendicular polarization configurations, respectively. Note that these room-temperature spectra do not allow us to detect the weakest features around the peak at $\sim 370 \text{ cm}^{-1}$ that were detected at 80 K. In any case, and as it is expected, the A_g and E_g modes can be easily identified because they have diagonal Raman tensors,[Todorov] and therefore they become extinct under perpendicular polarization. This is the case, for instance, of the sharp peak at $\sim 120 \text{ cm}^{-1}$, which is well-known to correspond to an A_g mode in most R_2O_3 sesquioxides.[Abrashv] Similarly, the peak at $\sim 148 \text{ cm}^{-1}$ can be unambiguously attributed to an E_g optical mode. In contrast, the intensity of F_g modes is barely changed with polarization, as is the case of several of the low-frequency modes that are visible in **Figs. 2 and 3**.

The polarized Raman spectra of **Fig. 3** also allow one to correctly locate the weak F_g peaks that appear at ~ 305 and $\sim 420 \text{ cm}^{-1}$, in good agreement with the DFT calculations using the PBEsol functional. On the other hand, these spectra indicate that the weak feature at $\sim 410 \text{ cm}^{-1}$ corresponds to an A_g mode, as also predicted by DFT calculations (see **Fig. 2** and **Table II**). This value is somewhat lower than that expected taking into account the values for the high-frequency A_g mode reported in Ref. [Abrashv] for the C-type R_2O_3 compounds (for instance, 425 cm^{-1} in Dy_2O_3 and 414 cm^{-1} in Gd_2O_3). This difference could be due to wrong symmetry assignment of this mode in some of the previous studies, especially in Gd_2O_3 . On the other hand, the spectra of **Fig. 3** seem to indicate that the peak at $\sim 325 \text{ cm}^{-1}$ has mainly contribution from an E_g mode, since the intensity of this peak almost vanishes under perpendicular polarization. However, the mode corresponding to this frequency region in other R_2O_3 compounds has been previously attributed to $F_g + E_g$ symmetry because of the possible proximity between one F_g mode and one E_g mode. [Abrashv] The present results, at least in the case of Tb_2O_3 , suggest that this peak has mainly E_g symmetry. And, clearly, the frequency of this mode is consistent with the values reported in other R_2O_3 compounds in this frequency region.[Abrashv]

As expected, the phonon frequencies measured in this work are consistent with the trends exhibited by the C-type R_2O_3 sesquioxides as a function of the unit cell parameter or equivalently the R-O cation-anion distance. The high-frequency phonons involving O vibrations show a clear monotonic upward frequency shift with decreasing the lattice parameter.[Abrashv] This result can be attributed to the fact that the effective spring constant associated with the different R-O bonds is enhanced when the interatomic distances are reduced,[Ubalini] which in turn is a consequence of the reduction of the ionic radius with increasing the number of f -electrons in the shell of the R cation. In contrast, the low-frequency phonons (i.e., those involving oscillations of the R cation, as seen in **Fig. 1** for the case of Tb_2O_3) have Raman frequencies that barely depend

on R because the upward frequency shift is counteracted by the increase of the atomic mass of R, except for Y_2O_3 and Sc_2O_3 . [Abrashv]

Finally, we would like to remark that several works have pointed out that the Raman-active mode frequencies of Eu_2O_3 exhibit a somewhat distinct behavior. The high-frequency Raman peaks of this compound tend to appear at frequencies that are sizably lower than the rest of R_2O_3 compounds when they are plotted as a function of the lattice parameter. [Abrashv] According to previous works, the softening of Eu_2O_3 modes could be related to the specific electronic configuration of Eu^{3+} relative to the rest of lanthanides, [Urban] but also to the presence of O vacancies in the crystal lattice of Eu_2O_3 . [Abrashv] In order to compare the lattice-dynamical properties of Tb_2O_3 with those of its neighboring R_2O_3 compounds and shed light on the anomalous behavior of Eu_2O_3 , we have performed additional first-principles lattice-dynamical calculations for the Raman-active modes of Eu_2O_3 , Sm_2O_3 , Gd_2O_3 and Dy_2O_3 with PBEsol functionals (see **Table III**). The results, plotted in **Fig. 4**, show that the high-frequency ($>300\text{ cm}^{-1}$) Raman-active modes of all these five compounds display a monotonic frequency decrease as a function of the lattice parameter (i.e., as a function of the ionic size of the cation). These data are in agreement with the general trend exhibited by the experimental data. [Abrashv] On the other hand, our calculations also show that the A_g Raman mode of Tb_2O_3 around 400 cm^{-1} must have a larger frequency than that of Gd_2O_3 , thus prompting for a revision of the anomalous value reported in Ref. [Abrashv] for this compound. Most remarkably, no softening of the high-frequency Raman modes is predicted by the present DFT-GGA calculations for Eu_2O_3 .

In this context, some authors have attributed the softening of the high-frequency optical modes of Eu_2O_3 (and also of Yb_2O_3) to the fact that the electron shells of Eu (and Yb) ions may be more deformable than those of other lanthanides due to the presence of shallow f -states. [Urban] Given the 3+ oxidation state of Eu in Eu_2O_3 , it is clear that such effect cannot be linked to the half-filled $4f^7$ configuration of the 2+ oxidation state, which is more stable than the $4f^6$ configuration of Eu^{3+} . Interestingly, the low-frequency modes of Eu_2O_3 , i.e. those actually involving Eu vibrations, do not display any sizable frequency change relative to the rest of R_2O_3 compounds. [Abrashv] This observation, together with the results of our DFT calculations (**Fig. 4**), suggest that the anomalous behavior of the high-frequency Raman modes of Eu_2O_3 is not related to its specific electronic configuration. Thus, it is likely that the presence of O vacancies in the crystal structure of Eu_2O_3 is responsible for the frequency reduction exhibited by some high-frequency Raman peaks of this compound. More investigations should be carried out to ascertain the origin of this effect and, in particular, if it is related to the growth process or even to a photoinduced Eu^{3+} to Eu^{2+} valence change of the Eu ions. The latter, which has been previously reported for Eu_2O_3 fine particle films under 325-nm laser light irradiation, [Mochi] could also explain the anomalous behavior of the Raman-active modes of this compound.

Conclusions

We have reported a joint experimental and theoretical study of the lattice dynamics of C-type Tb_2O_3 . Up to sixteen Raman-active modes have been measured in high-quality Tb_2O_3 single crystal. The comparison of experimental results with first-principles lattice dynamics calculations has allowed us to assign the symmetry of the experimentally observed Raman-active modes. We have shown that the zone-center Raman-active optical phonons of Tb_2O_3 follow the same trend as those of other RE and related sesquioxides with C-type or bixbyite structure. In this context, both our experimental Raman scattering measurements on Tb_2O_3 and our lattice dynamics calculations on Tb_2O_3 , Dy_2O_3 , Gd_2O_3 , Eu_2O_3 and Sm_2O_3 , which show a monotonic decrease of the Raman frequencies with increasing lattice parameter along the Tb_2O_3 - Gd_2O_3 - Eu_2O_3 - Sm_2O_3 - Dy_2O_3 series, prompt for a revision of the Raman spectra of Eu_2O_3 and also of some modes of Gd_2O_3 . More investigations are required in order to explain the anomalies reported in the literature for the high-frequency Raman-active modes of Eu_2O_3 .

Acknowledgements

This study was supported by the Spanish Ministerio de Economía y Competitividad under Projects MAT2015-71070-REDC, MAT2015-71035-R, MAT2016-75586-C4-2/3-P and FIS2017-2017-83295-P. A.M. and P.R.-H. acknowledge computing time provided by Red Española de Supercomputación (RES) and MALTA-Cluster.

References

- [JAP_2010] T.-M. Pan, F.-H. Chen, and J.-S. Jung, *J. Appl. Phys.* **108**, 074501 (2010).
- [TSF_2012] C. H. Kao, K. C. Li, M. H. Lee, S. N. Cheng, C. H. Huang, and W. K. Lin, *Thin Solid Films* **520**, 3402 (2012).
- [APL_2014] N. W. Gray, M. C. Prestgard, and A. Tiwari, *Appl. Phys. Lett.* **105**, 222903 (2014).
- [Geppert] I. Geppert, M. Eizenberg, N. A. Bojarczuk, L. F. Edge, M. Copel and S. Guha, *J. Appl. Phys.* **108**, 024105 (2010).
- [Belaya] S. V. Belaya, V. V. Bakovets, A. I. Boronin, S. V. Koshcheev, M. N. Lobzareva, I. V. Korolkov and P. A. Stabnikov, *Inorg. Mater.* **50**, 379 (2014).
- [Bakovets] V. V. Bakovets, S. V. Belaya, M. N. Lobzareva, and E. A. Maksimovskii, *Inorg. Mater.* **50**, 576 (2014).
- [CEC_2015] P. Veber, M. Velázquez, G. Gadret, D. Rytz, M. Peltz, and R. Decourt. *CrystEngComm* **17**, 492 (2015).
- [Abrashev] M. V. Abrashev, N. D. Todorov, and J. Geshev, *J. Appl. Phys.* **116**, 103508 (2014).
- [Irshad] K. A. Irshad, N. V. Chandra Shekar, T. R. Ravindran, V. Srihari, and K.K. Pandey, *Journal of Molecular Structure* **325**, 1128 (2017).
- [Urban] M. W. Urban and B. C. Cornilsen, *J. Phys. Chem. Solids* **48**, 475 (1987).
- [VASP] G. Kresse and J. Furthmüller, *Set. Comput. Mater. Sci.* **6**, 15 (1996).
- [PBE] J. P. Perdew, K. Burke, and M. Ernzerhof, *Phys. Rev. Lett.* **77**, 3865 (1996).
- [PBEsol] J. P. Perdew, A. Ruzsinszky, G. I. Csonka, O. A. Vydrov, G. E. Scuseria, L. A. Constantin, X. Zhou, and K. Burke, *Phys. Rev. Lett.* **100**, 136406 (2008).
- [García-Domene12] B. Garcia-Domene, H. M. Ortiz, O. Gomis, J. A. Sans, F. J. Manjón, A. Muñoz, P. Rodríguez-Hernández, S. N. Achary, D. Errandonea, D. Martínez-García, A. H. Romero, A. Singhal, and A. K. Tyagi, *J. Appl. Phys.* **112**, 123511 (2012).
- [Gomis14] O. Gomis, D. Santamaría-Pérez, J. Ruiz-Fuertes, J. A. Sans, R. Vilaplana, H. M. Ortiz, B. García-Domene, F. J. Manjón, D. Errandonea, P. Rodríguez-Hernández, A. Muñoz, and M. Mollar, *J. Appl. Phys.* **116**, 133521 (2014).
- [White] W.B. White and V. G. Keramidas, *Spec. Acta A* **28**, 501 (1972).
- [Kranert14] C. Kranert, R. Schmidt-Grund and M. Grundmann, *Phys. Stat. Sol. RRL* **1** (2014).
- [Todorov] N. D. Todorov, M. V. Abrashev, V. Marinova, M. Kadiyski, L. Dimowa, and E. Faulques, *Phys. Rev. B* **87**, 104301 (2013).
- [Zhong] H. Zhong, W. Cai, L. Zhang, *Mater. Res. Bull.* **34**, 233 (1999).
- [Silversmith] A. J. Silversmith, D. M. Boye, K. S. Brewer, C. E. Gillespie, Y. Lu, D. L. Campbell, *J. Lumin.* **121**, 14 (2006).

[Jinqiu] Y.U. Jinqiu, C.U.I. Lei, H.E. Huaqiang, Y.A.N. Shihong, H.U. Yunsheng, and W.U. Hao, *Journal of Rare Earths* **32**, 1 (2014).

[Ubaldini] A. Ubaldini and M. M. Carnasciali, *J. Alloys and Compounds* **454**, 374 (2008).

[Adachi] G. Adachi and N. Imanaka, *Chem. Rev.* **98**, 1479 (1998).

[Mochi] S. Mochizuki, F. Fujishiro, and K. Ishiwata, *Journal of Physics: Conference Series* **21**, 189 (2005).

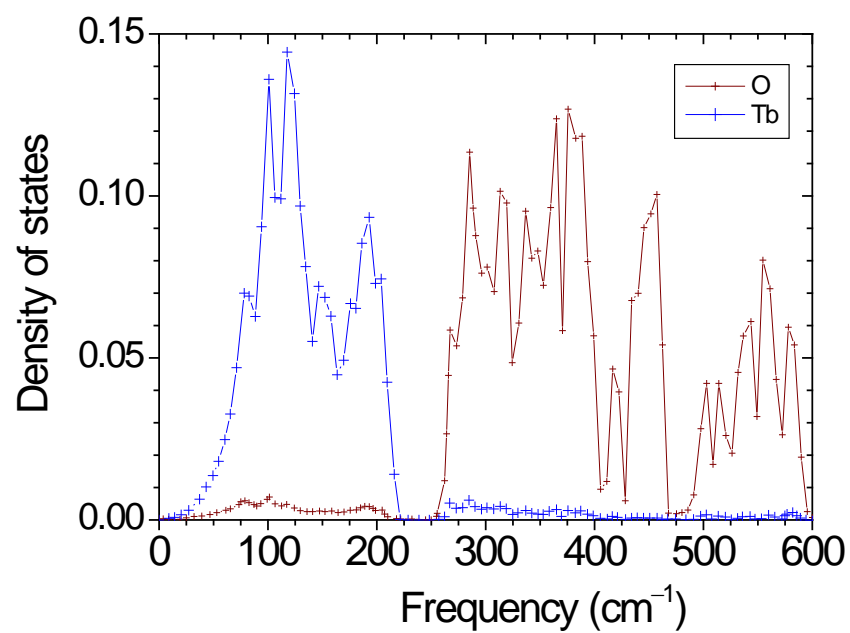


Fig. 1: Tb- and O-projected PDOS of Tb₂O₃ as obtained with first-principles DFT-GGA calculations using the PBEsol functional.

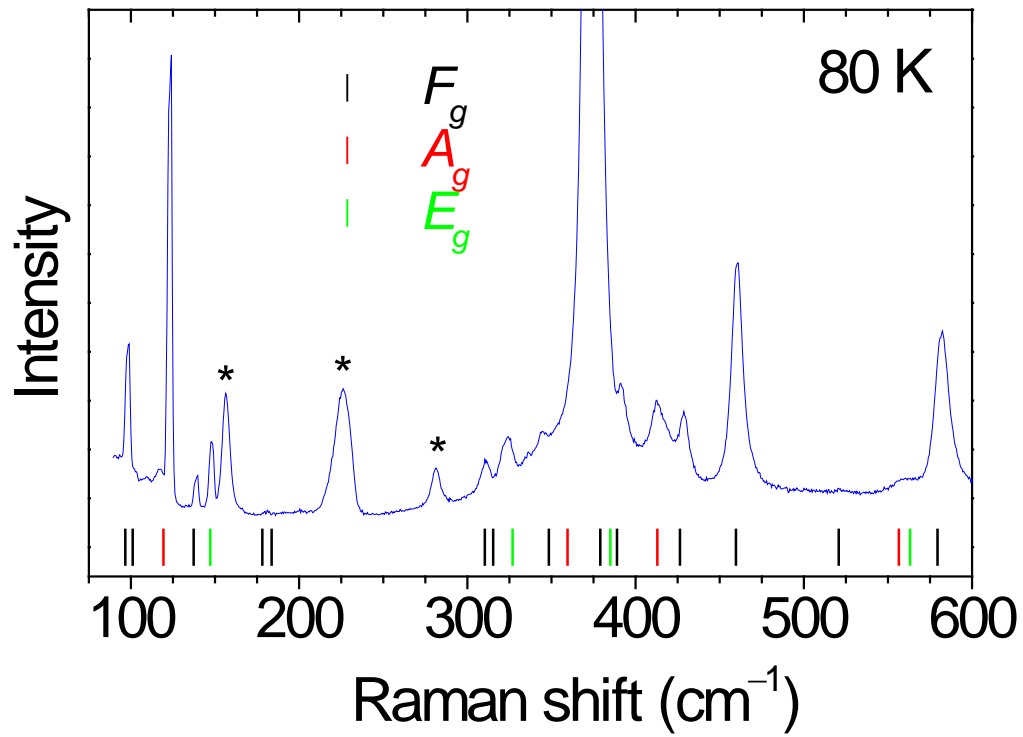


Fig. 2: Unpolarized Raman spectrum of Tb_2O_3 acquired at 80 K. Peaks marked with an asterisk are assigned to photoluminescence lines from Tb. In the bottom of the figure, the position of the vertical lines indicates the frequency of the Raman-active phonons of Tb_2O_3 (F_g , A_g and E_g symmetries) as obtained with first-principles DFT-GGA calculations using the PBEsol functional.

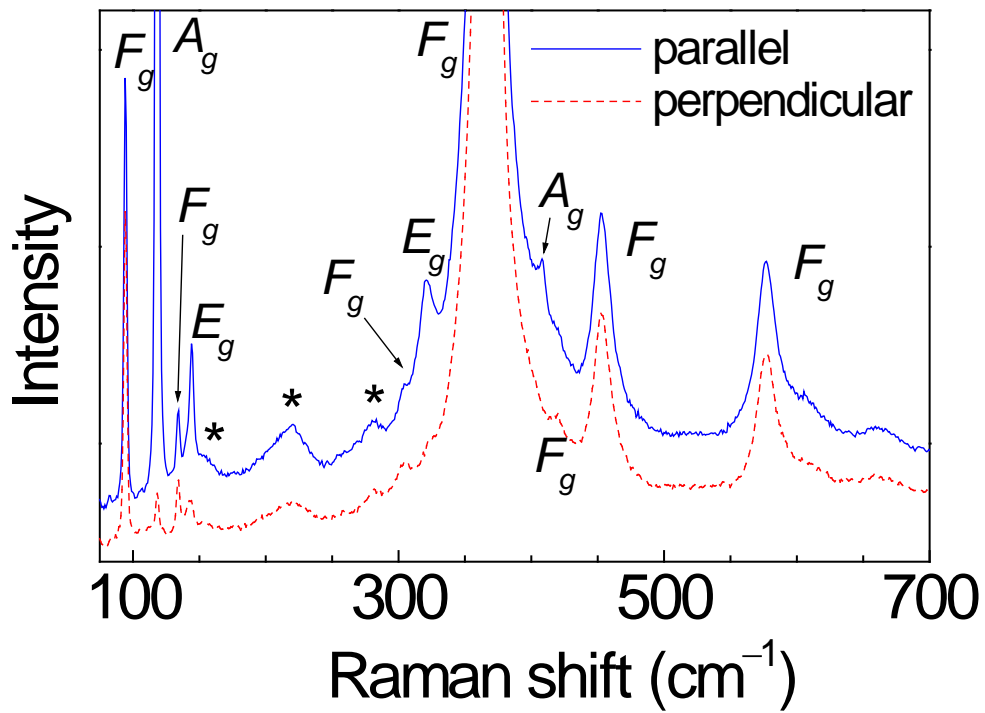


Fig. 3: Polarized Raman spectra of Tb₂O₃ acquired at room temperature with parallel and perpendicular polarization configurations. Peaks marked with an asterisk are assigned to photoluminescence lines from Tb.

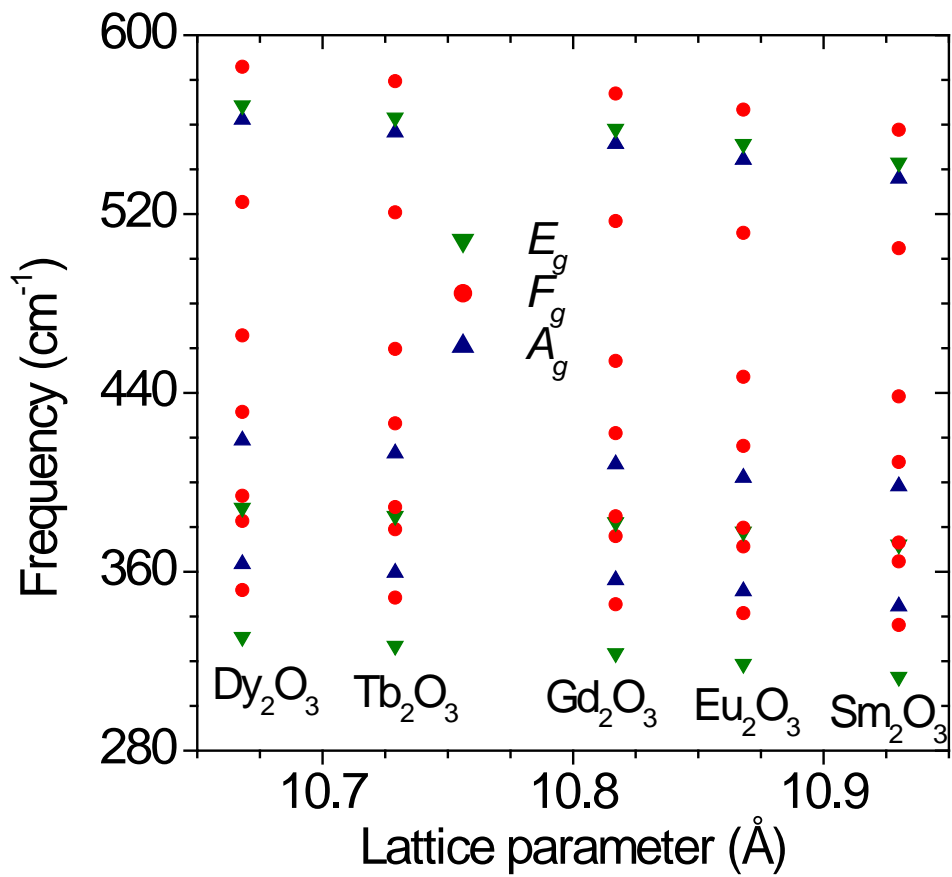


Fig. 4: Theoretical frequency values of the high-frequency Raman-active phonons of R_2O_3 compounds ($\text{R}=\text{Dy}, \text{Tb}, \text{Gd}, \text{Eu}, \text{Sm}$) as a function of the lattice parameter, as obtained with first-principles DFT-GGA calculations using PBEsol functionals.

	Exp. ^a	PBE	PBEsol
a_0 (Å)	10.732	10.748	10.623
B_0 (GPa)	-	139.21	151.24
B'	-	4.34	4.42

^aRef. [CEC_2015]

Table I. Experimental (Exp.) and theoretical lattice parameter (a_0), bulk modulus (B_0) and its pressure derivative (B') for Tb_2O_3 . Theoretical results obtained with DFT-GGA calculations using PBE and PBEsol functionals are given for comparison.

Symmetry	$\omega_{\text{PBE}}(\text{cm}^{-1})$	$\omega_{\text{PBEsol}}(\text{cm}^{-1})$	$\omega_{\text{exp.}}(\text{cm}^{-1})$
F_g^1	95.05	96.69	
F_g^2	98.36	101.05	98.1
A_g^1	114.29	119.33	123.4
F_g^3	132.35	137.31	139.0
E_g^1	143.13	147.16	148.1
F_g^4	171.36	178.15	
F_g^5	177.48	183.63	180.6
F_g^6	295.32	310.35	310.9
F_g^7	300.68	315.36	
E_g^2	311.07	326.86	324.1
F_g^8	330.57	348.42	345.3
A_g^2	345.04	359.55	
F_g^9	360.67	379.03	374.3
E_g^3	365.13	384.99	
F_g^{10}	372.74	388.90	391.5
A_g^3	396.77	412.95	413.3
F_g^{11}	411.15	426.37	428.9
F_g^{12}	442.06	459.65	460.4
F_g^{13}	505.15	520.73	521.5
A_g^4	541.45	556.49	
E_g^4	548.42	563.14	559.1
F_g^{14}	563.49	579.46	582.4

Table II. Experimental (at 80 K) and theoretical frequencies of the Raman-active modes in Tb_2O_3 . Theoretical frequencies obtained with DFT-GGA calculations using a PBE and a PBEsol functional are given for comparison.

Symmetry	Dy ₂ O ₃	Tb ₂ O ₃	Gd ₂ O ₃	Eu ₂ O ₃	Sm ₂ O ₃
F_g^1	99.81	96.69	96.21	96.51	95.16
F_g^2	104.43	101.05	100.51	100.76	99.30
A_g^1	122.94	119.33	119.11	119.84	116.70
F_g^3	141.22	137.31	137.20	138.37	137.27
E_g^1	151.48	147.16	146.90	147.98	146.75
F_g^4	183.31	178.15	177.99	179.52	178.19
F_g^5	188.95	183.63	183.46	185.07	183.66
F_g^6	314.44	310.35	307.33	303.16	297.11
F_g^7	319.64	315.36	312.03	307.47	300.93
E_g^2	330.85	326.86	323.55	318.80	312.95
F_g^8	351.82	348.42	345.49	341.50	336.22
A_g^2	363.43	359.55	356.26	351.36	344.55
F_g^9	382.69	379.03	375.94	371.36	364.61
E_g^3	388.58	384.99	382.16	377.94	372.18
F_g^{10}	393.95	388.90	384.81	379.71	373.09
A_g^3	418.77	412.95	408.06	402.10	398.29
F_g^{11}	431.46	426.37	422.00	416.26	409.09
F_g^{12}	465.71	459.65	454.26	447.18	438.47
F_g^{13}	525.36	520.73	516.86	511.60	504.74
A_g^4	562.20	556.49	551.39	544.33	535.84
E_g^4	568.61	563.14	558.13	551.31	542.99
F_g^{14}	585.86	579.46	573.92	566.68	557.66

Table III. Theoretical frequencies (in cm⁻¹) of the Raman-active modes in Dy₂O₃, Tb₂O₃, Gd₂O₃, Eu₂O₃ and Sm₂O₃ as obtained with DFT-GGA calculations using a PBEsol functional.